

# A WKB approach to scalar fields dynamics in curved space-time

J. Grain & A. Barrau<sup>1</sup>

*Laboratory for Subatomic Physics and Cosmology, Joseph Fourier University, CNRS-IN2P3,  
53, avenue de Martyrs, 38026 Grenoble cedex, France*

## Abstract

Quantum fields exhibit non-trivial behaviours in curved space-times, especially around black holes or when a cosmological constant is added to the field equations. A new scheme, based on the Wentzel-Kramers-Brillouin (WKB) approximation is presented. The main advantage of this method is to allow for a better physical understanding of previously known results and to give good orders of magnitude in situations where no other approaches are currently developed. Greybody factors for evaporating black holes are rederived in this framework and the energy levels of scalar fields in the Anti-de Sitter (AdS) spacetime are accurately obtained. Stationary solutions in the Schwarzschild-Anti-de Sitter (SAdS) background are investigated. Some improvements and the basics of a line of thought for more complex situations are suggested.

PACS: 11.15.Kc , 04.62.+v , 04.70.Dy

---

<sup>1</sup>corresponding author, email : Aurelien.Barrau@cern.ch

# 1 Introduction

The study of some of the most intriguing phenomena in our Universe, such as the evaporation of microscopic black holes or the parametric amplification of primordial quantum fluctuations, is performed within the framework of quantum field theory in curved space-time. Although well-established and reliable, as it does not require any quantization of the gravitational field itself, this theoretical framework leads to highly non-trivial partial differential equations whose resolution is, in most cases, based on numerical investigations. The Wentzel-Kramers-Brillouin (WKB) approximation and its extension to semi-classical methods (introduced by Kramers [1], Young & Uhlenbeck [2] and readdressed by Langer [3]) can be extremely useful to describe those physical systems.

The WKB method is used to approximately solve the following equation :

$$\left( \frac{d^2}{d\xi^2} + p^2(\xi) \right) \psi(\xi) = 0 \quad (1)$$

where the real function  $p^2$  can be either positive or negative valued. Nevertheless, WKB wave functions  $\tilde{\psi}$  are exact solutions of another differential equation :

$$\left( \frac{d^2}{d\xi^2} + p^2(\xi) \right) \tilde{\psi}(\xi) = \left( \frac{3}{4p^2} \left( \frac{dp}{d\xi} \right)^2 - \frac{1}{2p} \frac{d^2p}{d\xi^2} \right) \tilde{\psi}(\xi), \quad (2)$$

which restricts the validity of the approximation to regions where

$$|p^2| \gg \left| \frac{3}{4p^2} \left( \frac{dp}{d\xi} \right)^2 - \frac{1}{2p} \frac{d^2p}{d\xi^2} \right|. \quad (3)$$

It means that if the momentum is a linear function of  $\xi$ , the WKB wave function becomes an exact solution of Eq. (1). The WKB approximation can therefore provide very accurate results if the considered momentum squared is, depending on the potential, dominated by the constant, linear and quadratic terms in its Taylor expansion.

Recently, this approximation has been used to derive many important results about quantum fields propagating in a curved background. The Hawking evaporation process [4], as well as the inflationary cosmological perturbations [5, 6], have been investigated within this scheme. In Ref. [4], the Hawking temperature for a Schwarzschild black hole was rederived whereas, in Ref. [5], the spectral index and the amplitude of the inflationary perturbations were recovered nearly exactly. Finally, the WKB method has also been extensively used in order to determine

the quasi-normal frequencies of black holes (see Ref. [7] and Ref. [11]). The WKB tunnel probability used in the computation of the quasi-normal frequencies has also been applied to estimate the greybody factors for gravitons emitted by a  $D$ -dimensional Schwarzschild black holes [10].

In this article, we extend the idea of the WKB and semi-classical methods to the propagation of massless, minimally coupled, scalar fields in a static and spherically symmetric curved background, called Schwarzschild-like hereafter. Section 2 is devoted to the derivation of the radial part of the Klein-Gordon (KG) equation and to its rewriting in a Schrödinger-like form, such as Eq. (1). It is shown that this new equation is the quantum version of a slightly-modified relativistic Hamilton-Jacobi equation. The semi-classical scheme is applied to solve the problem and to derive the quantization rule and WKB tunnel probability. In Section 3, the discrete energy spectrum for massless scalar fields embedded in an Anti-de Sitter (AdS) Universe is derived and compared with the exact spectrum [8, 9]. In Section 4, the problem of the determination of the greybody factors, *i.e.* the coupling between quantum fields and black holes, is investigated. The emission/absorption cross-sections are thus determined for scalar fields evolving in a 4-dimensional Schwarzschild background. The resulting WKB cross-sections are also compared with the exact ones (and to those obtained in Ref. [10]). In Section 5, the propagation of scalar fields in a Schwarzschild-Anti-de Sitter (SAdS) space-time is addressed : it is shown that resonances, whose energies and bandwidths are obtained, arise in the state density. Finally, in Section 6, we draw up some conclusions and comments about the usefulness and reliability of the semi-classical approximation and underline some perspectives to improve this method. Some general arguments about its significance to study quantum fields in curved space-time are briefly given.

## 2 Scalar fields in Schwarzschild-like space-time

### 2.1 Equation of motion

A static and spherically symmetric space-time is described by the general Schwarzschild-like metric, totally determined by one function  $h(r)$  :

$$ds^2 = h(r)dt^2 - \frac{dr^2}{h(r)} - r^2 d\Omega^2 \quad (4)$$

where  $d\Omega$  is the solid-angle. The propagation of massless and minimally coupled scalar particles in this background is given by the solution of the KG equation  $\Phi_{;\mu}^{\mu} = 0$ . The field can be decomposed into eigenmodes of normal frequency  $\omega$  and angular momentum  $\ell$ ,  $\Phi(t, r, \Omega) = e^{-i\omega t} Y_{\ell}^m(\Omega) R(r)$ , the dynamics being totally given by the radial function  $R(r)$  which satisfies the radial part of the KG equation :

$$\frac{d}{dr} \left( hr^2 \frac{dR}{dr} \right) + \left( \frac{\omega^2 r^2}{h} - \ell(\ell + 1) \right) R = 0 \quad (5)$$

where  $\ell(\ell + 1)$  corresponds to the eigenvalues of the angular part of the KG equation.

The resolution of this equation strongly depends on the shape of the metric function  $h$  and it is usually not possible to obtain exact solutions, even in a simple background such as the Schwarzschild space-time. However, Eq. (5) can be modified by the use of the tortoise coordinate  $r^*$ , defined as  $dr^* = dr/h(r)$ , and a new radial function  $U(r) = rR(r)$ . It becomes of the Schrödinger type :

$$-\frac{d^2 U}{dr^{*2}} + \underbrace{h(r) \left( \frac{\ell(\ell + 1)}{r^2} + \frac{1}{r} \frac{dh}{dr} \right)}_{\mathcal{M}(r^*)} U = \omega^2 U, \quad (6)$$

which means that the square of the momentum operator  $i\partial/\partial r^*$  is equal to  $\omega^2 - \mathcal{M}(r^*)$ . We interpret Eq. (6) as the operational version of the classical Hamilton-Jacobi equation  $\mathcal{H}^2 = p^2 + V^2(r^*)$  where the  $\mathcal{M}$  function is identified to the square of a potential-like contribution. Except by the author of Ref. [14], the  $\mathcal{M}$  function is usually associated with  $V$  and not with  $V^2$  (see, *e.g.*, Ref. [11, 13]). Although this does not change the mathematical structure and the solutions, we prefer to identify  $\mathcal{M}$  function with the square of the potential in order to obtain a homogeneous classical Hamilton-Jacobi equation in a physically-consistant way. Eq. (6) can be regarded as the quantum version of the classical equation of motion for a test particle in a Schwarzschild background given by :

$$\left( \frac{dr}{d\tau} \right)^2 + h(r) \left( 1 + \frac{L^2}{r^2} \right) = E^2 \quad (7)$$

where the second term of the left hand side of the above equation is seen as the square of the potential. Consequently, the propagation of scalar fields in a Schwarzschild-like background is

based on a classical problem described by the action  $S$  solution of

$$\left(\frac{\partial S}{\partial r^*}\right)^2 + V^2(r^*) = \left(\frac{\partial S}{\partial t}\right)^2. \quad (8)$$

It should be noticed that the above equation slightly differs from the relativistic Hamilton-Jacobi equation for massless particles evolving in a spatial potential. Particles propagating in a spatial potential are described by the Lagrangian  $\mathcal{L} = -m\sqrt{1-v^2} - V(r^*)$  whereas the considered problem can be seen as a free particle with a mass which depends upon the position  $\mathcal{L} = -V(r^*)\sqrt{1-v^2}$ . Because Eq. (6) has exactly the same mathematical form as Eq. (1), the semi-classical approximation can be easily applied to the propagation of massless scalar fields in a Schwarzschild-like background, keeping in mind that the underlying classical problem is described by the above-mentioned Lagrangian.

## 2.2 Semi-classical approach

The quantum version of the Hamilton-Jacobi relation is given by the following KG-like equation :

$$\left(-\hbar^2 \frac{\partial^2}{\partial \xi^2} + V^2(\xi)\right) \psi(\xi, t) = -\hbar^2 \frac{\partial^2 \psi}{\partial t^2}(\xi, t). \quad (9)$$

In a Schwarzschild-like background, this equation corresponds to the time and radial part of the KG equation, the angular part being separated using spherical harmonics, with  $\xi$  standing for the tortoise radial coordinate and  $t$  for the Schwarzschild time. The  $U$  radial function of eq. 6 corresponds to the spatial part of the  $\psi$  wavefunction in the above equation. For an initial event  $\mathcal{I} = (t_i, \xi_i)$  and a final one  $\mathcal{F} = (t_f, \xi_f)$ , the ansatz corresponds to the sum over all the classical paths given by

$$\psi(\mathcal{F}, \mathcal{I}) = \sum_n F_n(\mathcal{F}, \mathcal{I}) e^{i \frac{S_n(\mathcal{F}, \mathcal{I})}{\hbar}}, \quad (10)$$

where  $S_n(\mathcal{F}, \mathcal{I})$  is the classical action of the  $n^{\text{th}}$  path between  $\mathcal{I}$  and  $\mathcal{F}$ . Performing the power expansion up to the linear order leads to :

$$\left\{ \begin{array}{l} i\hbar \left( 2 \frac{\partial S}{\partial \xi_f} \frac{\partial F}{\partial \xi_f} + \frac{\partial^2 S}{\partial \xi_f^2} F \right) \\ + \left( \left( \frac{\partial S}{\partial \xi_f} \right)^2 + V^2 \right) F \end{array} \right\} = \left\{ \begin{array}{l} i\hbar \left( 2 \frac{\partial S}{\partial t_f} \frac{\partial F}{\partial t_f} + \frac{\partial^2 S}{\partial t_f^2} F \right) \\ + \left( \frac{\partial S}{\partial t_f} \right)^2 F \end{array} \right\} \quad (11)$$

where the  $n$  indices have been dropped for simplicity. The resolution is not directly performed and an alternative set of equations should be used. The first order relation leads to :

$$\frac{\partial}{\partial \xi_f} \left( |F|^2 \frac{\partial S}{\partial \xi_f} \right) - \frac{\partial}{\partial t_f} \left( |F|^2 \frac{\partial S}{\partial t_f} \right) = 0. \quad (12)$$

Considering Eq. (12) as an equation of continuity, we can define the quadri-current at the semi-classical order as  $|F|^2 p_\mu$ , so that :

$$- |F|^2 p_\mu = i (\psi \partial_\mu \psi^\dagger - \psi^\dagger \partial_\mu \psi). \quad (13)$$

For a stationary problem, *i.e.*  $\partial^2 \psi / \partial t^2 = -\omega^2 \psi$ , it is more convenient to consider a path with fixed energy and the Green function of the propagator is preferred. Using the stationary phase approximation, it is shown that, as in non-relativistic quantum mechanics, the Green function takes the form

$$G(\xi_f, \xi_i, \omega) = \sum_n \sqrt{\frac{p_n(\xi_i)}{p_n(\xi_f)}} e^{i \int_{\xi_i}^{\xi_f} p_n(\xi) d\xi}, \quad (14)$$

where  $p_n = \frac{\partial S_n}{\partial \xi}$ , corresponds to the classical momentum  $\sqrt{\omega^2 - V^2(\xi_f)}$  at the energy  $\omega$  and does not depend upon the considered path. Although most non-relativistic quantum results can be easily adapted, we have carefully checked, thanks to an explicit calculation of the density of states, that the Bohr-Sommerfeld quantization rule in a well-potential is recovered :

$$2 \int_{\xi_-(\omega_n)}^{\xi_+(\omega_n)} p_n(\xi, \omega_n) d\xi = (2n + 1) \pi, \quad (15)$$

where  $n$  is an integer and  $\xi_\pm$  the two turning points. Following the techniques of Ref. [16] (the classical action is here allowed to become complex) and using the matching procedure at the turning point described in appendix A, the transmission coefficient at the WKB order is found to be

$$|A|^2 = \exp \left( -2 \int_{\xi_-}^{\xi_+} p'(\xi, \omega) d\xi \right) \quad (16)$$

where the interval  $[\xi_-, \xi_+]$  corresponds to the region where energy of the particle is lower than the potential.

### 3 Energy spectrum in AdS Universe

#### 3.1 Exact results

It was shown in [8] that massless scalar fields, minimally coupled to gravity, propagating in an AdS space-time exhibit a discrete energy spectrum. We will briefly rederive those exact results using another –less rigorous– approach to compare them with semi-classical computations. For scalar particles propagating in a pure AdS space-time, the following Schwarzschild-like metric has to be considered :

$$ds^2 = \left(1 + \frac{r^2}{R^2}\right) dt^2 - \frac{dr^2}{\left(1 + \frac{r^2}{R^2}\right)} - r^2 d\Omega^2 \quad (17)$$

where  $R = (-\Lambda/3)^{1/2}$  is the curvature radius of the AdS space-time. The KG equation is solved [9] using a more convenient coordinate system [17, 18] :

$$\tau = \frac{t}{R} ; \rho = 2 \arctan \left( \frac{r}{R} + \sqrt{1 - \frac{r^2}{R^2}} \right) - \frac{\pi}{2} ; ds^2 = \frac{R^2}{\cos^2(\rho)} (d\tau^2 - d\rho^2 - \sin^2(\rho) d\Omega^2) . \quad (18)$$

With the ansatz  $\Phi(\tau, \rho, \Omega) = e^{-i\nu\tau} Y_\ell^m(\Omega) R(\rho)$ , the following radial equation is obtained :

$$\frac{\cos^2(\rho)}{\sin^2(\rho)} \frac{d}{d\rho} \left( \frac{\cos^2(\rho)}{\sin^2(\rho)} \frac{dR}{d\rho} \right) + \left( \nu^2 - \frac{\ell(\ell+1)}{\sin^2(\rho)} \right) R = 0 \quad (19)$$

which leads –see appendix B– to :

$$R(\rho) = \sin^\ell(\rho) \cos^3(\rho) P_{(\nu-\ell-3)/2}^{(\ell+1/2, 3/2)}(\cos(2\rho)) . \quad (20)$$

This solution, based on Jacobi polynomial, leads to the energy spectrum

$$(\omega_{n,\ell})_{(n,\ell) \in \mathbb{N}^2} = \left( \frac{2n + \ell + 3}{R} \right)_{(n,\ell) \in \mathbb{N}^2} \quad (21)$$

where a zero point energy clearly appears. The curvature of space-time,  $1/R$ , provides a natural unit for scalar particles energy and this quantization can be viewed as periodic conditions since the geodesics are closed in the AdS Universe.

#### 3.2 The Bohr-Sommerfeld quantization rule

The above results are a direct consequence of the quantum nature of the fields combined with the intrinsic curvature of the AdS Universe. Rewriting the radial part of the KG equation in

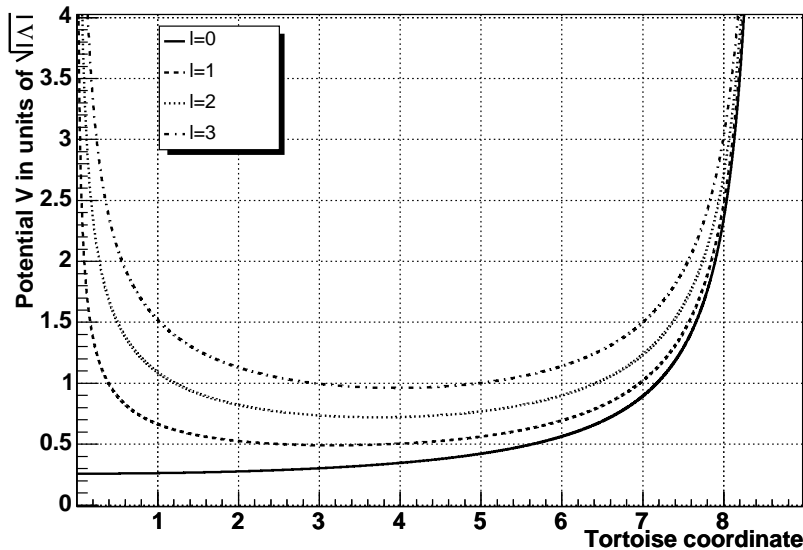


Figure 1: Potential seen by a scalar field in AdS space-time in units of  $\sqrt{|\Lambda|}$ .

a Schrödinger-like form, as mentioned in section 2.1, it is clear that the potential seen by a scalar particle is a well-potential for all the values of the orbital momentum but zero. This is illustrated in Fig. 1 and given by

$$V_\ell^2(r^*) = \frac{1}{R^2 \cos^2(r^*/R)} \left( \frac{\ell(\ell+1)}{\tan^2(r^*/R)} + 2 \right) \quad (22)$$

where the tortoise coordinate  $r^* = R \arctan(r/R)$  lies in the range  $[0, \pi R/2[$ . As a consequence, scalar fields clearly have to exhibit a discrete energy spectrum at variance to what happens in an asymptotically flat Universe. Moreover, the Bohr-Sommerfeld quantization method can be applied in order to determine the energy levels and compared with the exact results.

### 3.2.1 The $\ell = 0$ case

The  $\ell = 0$  case is first considered as some analytical calculations can be performed. The two turning points are  $r_-^* = 0$  and  $r_+^* = R \arctan\left(\sqrt{\frac{\omega^2 R^2 - 2}{2}}\right)$  and the potential takes the following form  $V_0(r^*) = \frac{\sqrt{2}}{R \cos(r^*/R)} + \delta(r^*)$ , where a Dirac distribution was included so as to take into account that the negative  $r^*$  region is forbidden. When one of the walls is infinitely steep, as is the case here, the Bohr-Sommerfeld quantization rule is slightly modified because of the new boundary conditions for the wave function [15]. The quantization rule reads in this case



$W_0 = (2n + \frac{3}{2})\pi$ . To account for the distribution involved, a more rigorous definition of this quantity shall be used :

$$W_0 = 2 \lim_{\varepsilon \rightarrow 0} \int_{r_-^* + \varepsilon}^{r_+^* - \varepsilon} \sqrt{\omega^2 - V^2(r^*)} dr^*. \quad (23)$$

We finally obtain the following value for the classical action  $W_0 = \pi(\omega R - \sqrt{2})$  which yields to the following spectrum for the  $\ell = 0$  case :

$$(\omega_{n,0})_{n \in \mathbb{N}} = \left( \frac{2n + \sqrt{2} + 3/2}{R} \right)_{n \in \mathbb{N}}. \quad (24)$$

The spectrum dependence with respect to the integer  $n$  is well recovered and, as a consequence, so are the energy gaps. Nevertheless, the zero point energy slightly differs from the accurate one : the semi-classical approach provides  $\omega_{0,0} = (3/2 + \sqrt{2})/R \simeq 2.91/R$  instead of  $3/R$ . This shift is due to the specific behaviour of the potential at  $r^* = 0$  leading to a high departure from any quadratic approximation. It is important to mention that if an infinite wall was not added, the quantization rule would follow Eq. (15), yielding to an energy spectrum which misestimates the zero point energy by 20% because the potential, if viewed as a function of the two variables  $(r^*, \ell)$ , is not continuous at  $(0, 0)$ .

### 3.2.2 The $\ell \neq 0$ case

For  $\ell > 0$ , the analytical computation of  $W_0(\omega)$  is not possible and numerical investigations have to be performed. To evaluate the energy levels, the equation

$$W_0(\omega, \ell) - (2n + 1)\pi = 0 \quad (25)$$

is numerically solved.  $W_0$  has to be rewritten in a more convenient way using the  $y = \tan(r^*/R)$  coordinate :

$$W_0 = 2 \int_{y_-}^{y_+} \frac{1}{1 + y^2} \sqrt{\omega^2 R^2 - (1 + y^2) \left( \frac{\ell(\ell + 1)}{y^2} + 2 \right)} dy \quad (26)$$

where  $y_{\pm}$  are the two turning points, determined in appendix C,

$$y_{\pm} = \frac{1}{2} \sqrt{\omega^2 R^2 - 2 - \ell(\ell + 1) \pm \sqrt{(2 + \ell(\ell + 1) - \omega^2 R^2)^2 - 8\ell(\ell + 1)}}. \quad (27)$$

The numerical results are presented on Fig. 2 and Fig. 3 where the energy levels  $\omega_{n,\ell}$  and the relative errors  $\Delta\omega/\omega$  are displayed respectively as a function of the integer  $n$  and as a function

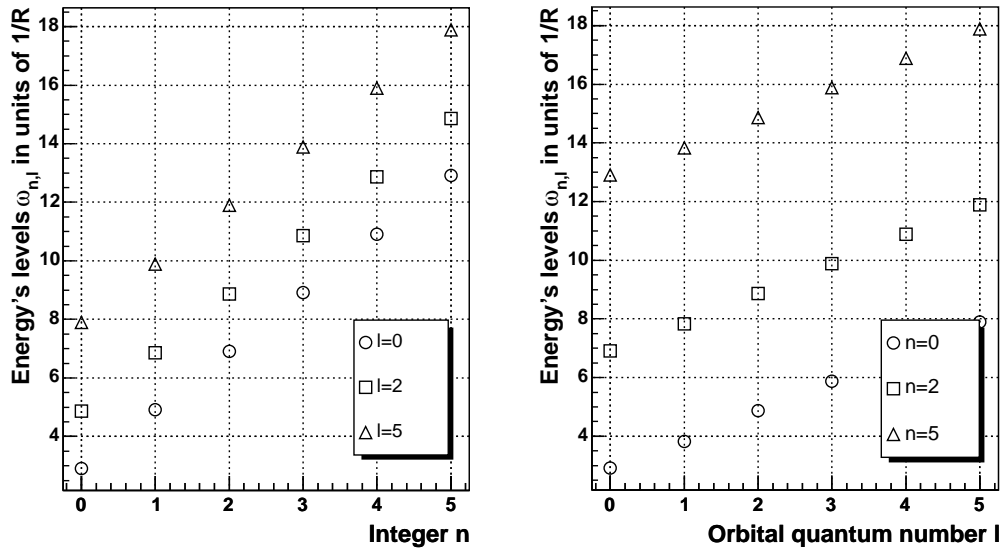


Figure 2: *left panel* : Energy levels as a function of the integer  $n$ . *Right panel* : Energy levels as a function of the orbital quantum number  $\ell$ . All the energies are expressed in units of  $R^{-1}$ .

of the orbital quantum number  $\ell$ . Although slightly underestimated, the energy levels are well recovered and the precision of this semi-classical approach increases with  $n$  and  $\ell$  : the total relative error remains below 5%. For a vanishing orbital quantum number, the result of the previous analytical calculation is recovered, as it should be. When  $\ell \neq 0$ , the energy levels as a function of the angular momentum are well described by a linear function with a  $\ell$ -intercept equal to  $(2n + 3)/R$ . Recovering the correct zero-point energy by taking the  $\ell \rightarrow 0$  limit lights up the particular behaviour of the potential for a vanishing angular momentum and confirms the prescription used in the previous section.

There are two possible sources of error in those numerical computations. The first one is due to numerical approximations and was checked to remain totally negligible. The second one is related to the Bohr-Sommerfeld quantization scheme which gives exact results up to the second order in the potential only. This error decreases both with  $n$  and with the orbital quantum number  $\ell$  : for a fixed value of  $n$ , not only does the energy levels increase with  $\ell$  but also does the minimum of the potential  $V_{min} = \left(\sqrt{2} + \sqrt{\ell(\ell + 1)}\right) R^{-1}$ . This result is expected as particles with higher energies are closer to “classicality”.

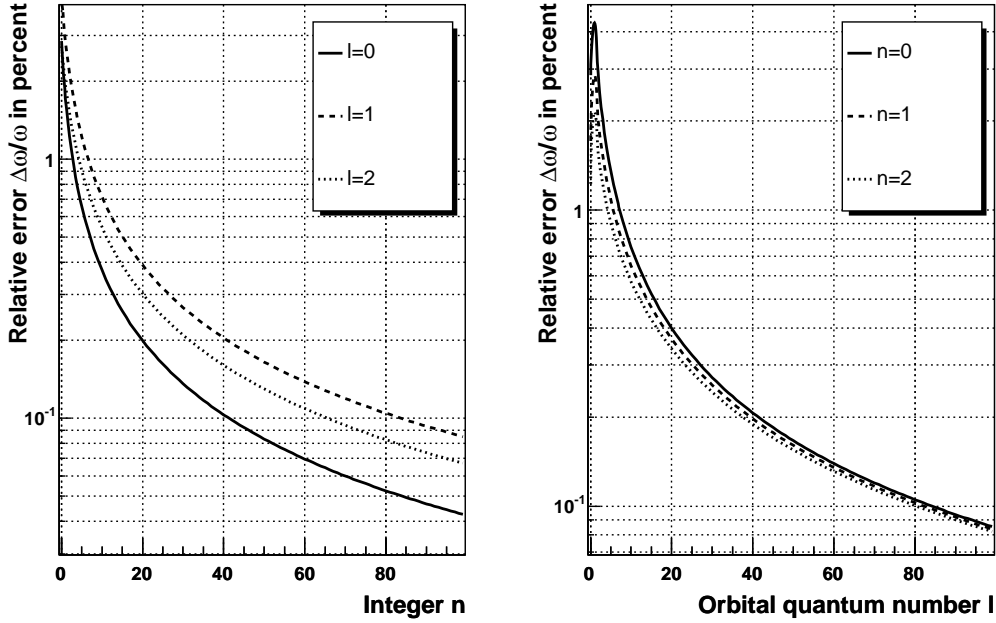


Figure 3: *left panel* : Total relative error  $\frac{\Delta\omega}{\omega}$  as a function of the integer  $n$ . *Right panel* : Total relative error  $\frac{\Delta\omega}{\omega}$  as a function of the orbital quantum number  $\ell$ .

## 4 Greybody factors for Schwarzschild black holes

For massless scalars, the flux emitted by an evaporating black hole can be written as [21] :

$$\frac{d^2 N}{d\omega dt} = \frac{4\pi\sigma_g(\omega)\omega^2}{e^{\frac{\omega}{T_{BH}}} - 1}. \quad (28)$$

The non trivial part mostly lies in the determination of the greybody factors  $\sigma_g(\omega)$  (related with the probability for an emitted particle to escape form the gravitational potential) whose computation involves the resolution of the KG equation, given by Eq. (5), in the Schwarzschild background. The tunnel probability  $|A_\ell|^2$  [22] yields to the greybody factors via the optical theorem [23] :

$$\sigma_g(\omega) = \sum_{\ell} \frac{(2\ell + 1)\pi}{\omega^2} |A_\ell|^2. \quad (29)$$

Unlike the AdS case, the intricate shape of the metric function describing Schwarzschild black holes does not allow for an analytical resolution of Eq. (5). As a consequence, all the evaluations of the greybody factors, from usual Schwarzschild black holes to  $D$ -dimensional Gauss-Bonnet ones [22, 24, 25, 26], are based on numerical investigations; thought some an-

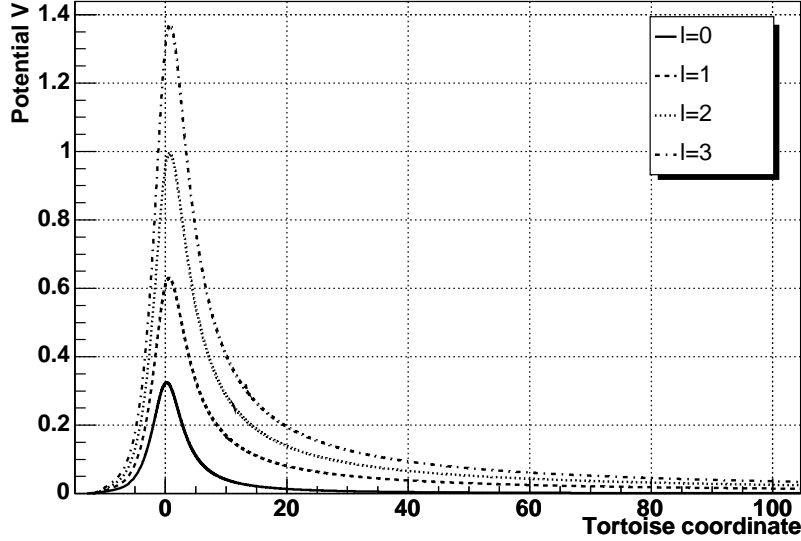


Figure 4: Potential seen by a scalar field propagating in Schwarzschild space-time

alytical methods can be applied in the high and low energy regimes [27]. However, using the WKB method, some approximated results can be obtained without big numerical codes. The aim of this study is to derive the greybody factors for 4-dimensional Schwarzschild black holes at the WKB order and to compare them with the exact results.

#### 4.1 WKB wave function and tunnel probability

For a black hole with a horizon radius  $r_H$ , we consider the metric :

$$ds^2 = \left(1 - \frac{r_H}{r}\right) dt^2 - \frac{dr^2}{1 - \frac{r_H}{r}} - r^2 d\Omega^2. \quad (30)$$

In the tortoise coordinates system  $(t, r^*)$ , particles are described by a wave function  $U$  evolving in the potential  $V$  (see Fig. 4) :

$$V_\ell^2(r) = \left(1 - \frac{r_H}{r}\right) \left(\frac{\ell(\ell+1)}{r^2} + \frac{r_H}{r^3}\right); \quad r^* = r + r_H \ln(r - r_H). \quad (31)$$

As it can be seen from Fig. 4, this potential tends to zero when  $r^* \rightarrow \pm\infty$ , making the use of the optical theorem valid. We define  $r_{\max}^*$  as the tortoise coordinate corresponding to the maximum value  $V_{\max}$ .

To determine the wave function, the "no-incoming wave at spatial infinity" hypothesis is used as there are no sources of particles far from the black hole. For particles with energies always greater than the potential, the wave function reads  $U(r^*) = A_{out} \exp\left(i \int_{r_0^*}^{r^*} p(x) dx\right)$  with  $p = \sqrt{\omega^2 - V^2}$ . For particles with energies lower than  $V_{max}$ , the space is divided into three regions  $\mathcal{A}$ ,  $\mathcal{B}$  and  $\mathcal{C}$ , corresponding respectively to  $] -\infty, r_-^*]$ ,  $[r_-^*, r_+^*]$  and  $[r_+^*, +\infty[$ , with  $(r_-^*, r_+^*)$  representing the two turning points. With the above boundary conditions, the wave function admits the following asymptotic regime :  $U(r^*) \simeq A_{in} \exp(-i\omega r^*) + A_{out} \exp(i\omega r^*)$  when  $r^* \rightarrow -\infty$  and  $U(r^*) \simeq B_{out} \exp(i\omega r^*)$  when  $r^* \rightarrow +\infty$ . The WKB wave function must therefore be read as :

$$U(r^*) = \begin{cases} \frac{1}{\sqrt{p(r^*)}} \left( A_{in} e^{-i \int_{r_1^*}^{r^*} p(x) dx} + A_{out} e^{i \int_{r_1^*}^{r^*} p(x) dx} \right) & \text{in region } \mathcal{A} \\ \frac{A_{evn}}{\sqrt{p'(r^*)}} e^{-\int_{r_1^*}^{r^*} p'(x) dx} & \text{in region } \mathcal{B} \\ \frac{B_{out}}{\sqrt{p(r^*)}} e^{i \int_{r_2^*}^{r^*} p(x) dx} & \text{in region } \mathcal{C} \end{cases} \quad (32)$$

with  $p$  and  $p'$  defined as in section 2.2. The above solutions show that particles in region  $\mathcal{A}$  are described by both incoming waves, *i.e* particles emitted by the black hole, and outgoing ones, *i.e* particles reflected on the potential barrier, whereas they are only described by outgoing waves in region  $\mathcal{C}$ . In region  $\mathcal{B}$ , particles are only described by evanescent waves as there are no sources of particles at spatial infinity. Using the procedure described in appendix A to match the different solutions at the two turning points, it is found that  $A_{in} = e^{-i\pi/2} A_{out}$  and  $B_{out} = e^{-\tau} A_{out}$  with  $\tau = \int_{r_-^*}^{r_+^*} p'(x) dx$ . This approach leads to a new understanding of the evaporation process.

Unlike the AdS case, it is not possible to inverse the relation  $r^* = f(r)$  and an explicit expression of the potential as a function of  $r^*$  cannot be found. However, the determination of the two turning points  $r_{\pm}^*$  as well as  $r_{max}^*$  can be performed using  $r$  as a variable instead of  $r^*$ . The tunnel probability is given by the ratio of the outgoing flux  $\mathcal{F}_U = i(U\partial_{r^*}U^\dagger - U^\dagger\partial_{r^*}U)$  at spatial infinity to the one at the event horizon of the black hole. Once reexpressed using the usual radial coordinate, the tunnel probability  $|\tilde{A}_\ell|^2$  is given by :

$$|\tilde{A}_\ell|^2 = \begin{cases} 1 & \text{if } \omega > V_{max} \\ e^{-2 \int_{r_-^*}^{r_+^*} \frac{\sqrt{V^2(r) - \omega^2}}{h(r)} dr} & \text{if } \omega < V_{max} \end{cases} \quad (33)$$

where  $r_{\pm}$  are the two turning points and  $V_{max}$  is obtained by computing the value of the

potential at  $r_{\max}$  so that

$$r_{\max} = \begin{cases} \frac{4}{3}r_H & \text{for } \ell = 0 \\ \frac{r_H}{4\ell(\ell+1)} \left( \frac{3\ell(\ell+1) - 3}{+\sqrt{9 + 9\ell^2(\ell+1)^2 + 14\ell(\ell+1)}} \right) & \text{for } \ell \neq 0. \end{cases} \quad (34)$$

Although the maximum value of the potential is analytically determined, the two turning points as well as the integral involved in the calculation of the tunnel probability have to be numerically computed. The above tunnel probability has to be linked with the transmission probability  $|A_\ell|^2$ , which is obtained using the flux for the  $R$  function  $\mathcal{F}_R = i(hr^2)(r^{-2}R\partial_r r^2 R^\dagger - r^{-2}R^\dagger\partial_r r^2 R)$ . As  $R(r) = U(r)/r$ , the usual radial wave function  $R$  is composed of incoming and outgoing spherical waves with amplitudes equal to the ones of the  $U$  function and the transmission probability  $|A_\ell|^2$  is given by  $|B_{out}/A_{out}|^2 = |\tilde{A}_\ell|^2$ . The WKB tunnel probability  $|\tilde{A}_\ell|^2$  can therefore be directly used in Eq. (29) to compute the value of the greybody factor.

## 4.2 Results for the cross-section and radiation spectra

Figure. 5 shows, on the left panel, the WKB emission/absorption cross-section alongside the exact one [22], numerically obtained [25], and, on the right panel, the relative error. We expect the WKB method to break down twice : in the low energy region because this is where the quantum nature of particles dominates and near the resonances, *i.e*  $\omega = V_{\max}$ , because the two turning points are extremely close one to the other. This behaviour can be seen by looking at the shape of the emission/absorption cross-section. The divergence is due to the  $\ell = 0$  partial wave whose transition probability tends to  $e^{-4\sqrt{r_H}}$  when  $\omega$  tends to zero. On the other hand, the cross-section at resonances, occurring when the energy of the field is equal to  $V_\ell$ , is overestimated in the WKB approach (although the spectrum is quite well recovered). The misestimation at resonances is not dramatic and leads to regular peaks in the relative error whose amplitude does not exceed 35%. Furthermore, it has only small consequences on the radiation spectrum. However, without the help of an exact calculation, the WKB approximation seems –as expected– hazardous to provide reliable results in the low-energy region. It is both due to the unavoidable behaviour of the turning points and to the huge steps for the tortoise coordinate numerically occurring close to the event horizon.

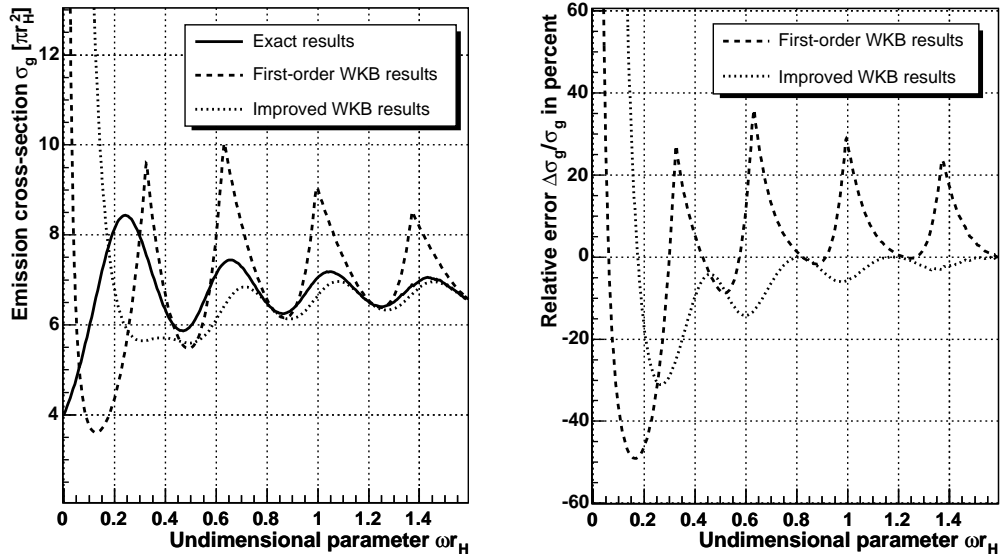


Figure 5: *Left panel* : Emission cross-section for a 4–dimensional Schwarzschild black hole. The solid line corresponds to exact numerical results, the dashed line to the first-order WKB approximation results and the dotted line to the improved WKB results. *Right panel* : Relative error  $\Delta\sigma_g/\sigma_g$  of the WKB cross-section estimation. The dashed line stands for the first-order WKB error and the dotted one to the improved WKB error.

In spite of this drawback, the WKB techniques provides good results in the intermediate and high energy regimes. First, the high energy optical limit is well recovered, as it can be seen on Fig. 5. Moreover, it was demonstrated in Ref. [10] that if the transmission coefficient  $|\mathcal{A}_\ell|^2$  tends to unity when  $\omega$  tends to infinity for all the partial waves, then the emission/absorption cross-section should tend to the optical limit when  $\omega \rightarrow +\infty$ . Our WKB transmission coefficient is in agreement with the above conditions and the cross-section has to tend to  $\sigma_g^{(\text{opt})} = 27\pi r_H^2/4$ . In the intermediate energy regime, the relative error admits an average value of 10% and decreases for higher values of the energy.

Those results could be improved using higher order semi-classical expansions. A third-order WKB tunnel probability has been derived by Iyer & Will and extended to the sixth order by Konoplya (see Ref. [11]) to derive the quasi-normal frequencies of black holes. It is optimised for resonant scattering near the top of the potential barrier and allows for a non-vanishing reflexion coefficient for particles with an energy greater than the maximum of the potential. This should allow to avoid the spiky structure at resonances. The transmission coefficient, successfully used to derive the greybody factors for gravitons emitted by  $D$ –dimensional Schwarzschild black

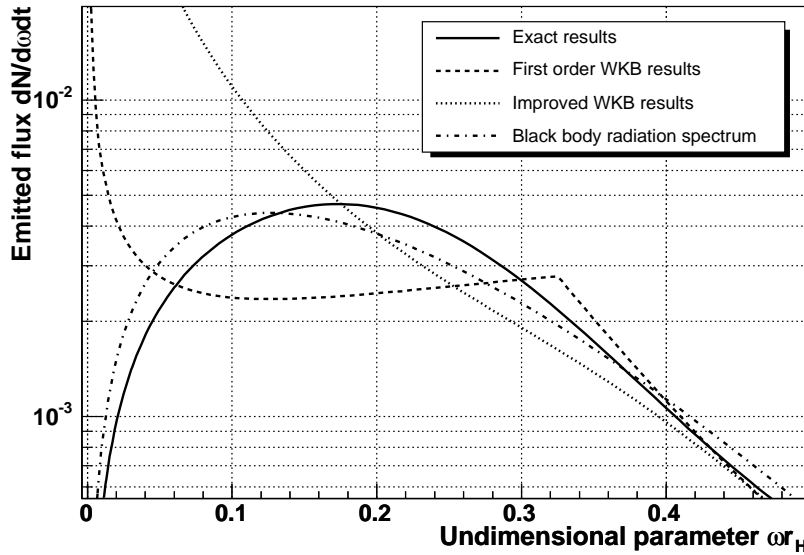


Figure 6: Scalar radiation spectrum from a 4–dimensional Schwarzschild black hole. The solid line corresponds to exact numerical results, the dashed one to the first-order WKB approximation results, the dotted line to the improved WKB results and the dashed-dotted one to a black body radiation spectrum with the high energy limit of the cross-section.

holes [10], takes the following form

$$|\mathcal{A}_\ell|^2 = \frac{1}{1 + e^{2i\pi(\nu+1/2)}} , \quad \nu + 1/2 = ip^2(r_{\max}) \left( 2 \frac{d^2 p^2}{dr^{*2}}(r_{\max}) \right)^{-1/2} . \quad (35)$$

The greybody factors obtained with the improved WKB tunnel probability are displayed on Fig. 5 where it can be seen that the breakdown of the approximation at the top of the potential barrier is removed. However, the infrared divergence cannot be avoided with this new technique, as is the case for gravitons [10].

The emission/absorption cross-section does not correspond to any physical quantity. The meaningful flux, or radiation spectrum, is displayed on Fig. 6. As it can clearly be seen, both WKB approximations allow for a good estimation of the high energy tail of the distribution whereas the low energy one is mis-estimated due to the infrared divergence. It should be pointed out that the WKB technique for the estimation of greybody factors is more of theoretical interest : it allows a first and fast estimation of the emission/absorption cross-section in both the intermediate and high energy regime (which is highly relevant to understand the consequences of the possibly intricate metric), but does not provide any real improvement in the determination



of the "experimental" spectrum.

## 5 Scalar fields in SAdS space-times

### 5.1 Shape of the potential

Fields in SAdS space-times have been intensively studied for quasi-normal modes estimation (see Ref. [11, 12] and references therein). Nevertheless, the general behaviour of scalar fields in those space-times has not been investigated and this study is carried out at the semi-classical order hereafter. SAdS space-times are described by a Schwarzschild-like metric with

$$h(r) = 1 - \frac{2M}{r} + \frac{r^2}{R^2}. \quad (36)$$

The black hole horizon radius corresponds to the positive real root of  $h(r)$  :  $2M = r_H(1 + r_H^2/R^2)$ . The potential seen by a scalar field and the tortoise coordinate are given by

$$\begin{aligned} V_\ell^2(r) &= \left(1 - \frac{2M}{r} + \frac{r^2}{R^2}\right) \left(\frac{\ell(\ell+1)}{r^2} + \frac{2M}{r^3} + \frac{2}{R^2}\right) ; \\ r^* &= R^2 \left[ \frac{r_H}{3r_H^2 + R^2} \ln \left( \frac{r - r_H}{\sqrt{r^2 + rr_H + r_H^2 + R^2}} \right) \right. \\ &\quad \left. + \frac{3r_H^2 + 2R^2}{(3r_H^2 + R^2)\sqrt{3r_H^2 + 4R^2}} \arctan \left( \frac{2r + r_H}{\sqrt{3r_H^2 + 4R^2}} \right) \right]. \end{aligned} \quad (37)$$

The shape of the potential strongly depends upon  $\eta = r_H/R$ . If  $\eta$  is much smaller than one, the black hole horizon radius is smaller than the characteristic AdS curvature radius, while if  $\eta$  is much greater than one, the horizon radius becomes greater than the curvature radius. The potential is depicted on Fig. 7 for  $\eta \ll 1$  and is a mixing of the potentials in Schwarzschild space-time and in AdS space-time : when  $r^* \rightarrow -\infty$ , *i.e.*  $r \rightarrow r_H$ , the potential falls down to zero because of the event horizon whereas it diverges to  $+\infty$  when  $r^* \rightarrow r_{\text{SAdS}}^*$ , *i.e.*  $r \rightarrow +\infty$ , where  $r_{\text{SAdS}}^* = \frac{R^2(3r_H^2 + 2R^2)}{(3r_H^2 + R^2)\sqrt{3r_H^2 + 4R^2}} \frac{\pi}{2}$ . It also exhibits a finite barrier -because of the presence of the black hole- for any value of the orbital quantum number  $\ell$ , which leads to the appearance of a local maximum  $V_{\text{max}}^{(\ell)}$  and minimum  $V_{\text{min}}^{(\ell)}$ , respectively located at  $r_{\text{max}}^*$  and  $r_{\text{min}}^*$ .

When  $\eta \gg 1$ , the finite potential barrier is present only at high values of the angular momentum : as examples, the barrier appears at  $\ell \simeq 10$  for  $\eta = 1$  and at  $\ell \simeq 10^6$  for  $\eta = 2$ . In the following, we will focus on the high hierarchy case ( $\eta \ll 1$ ) since it corresponds to the most physically interesting one.

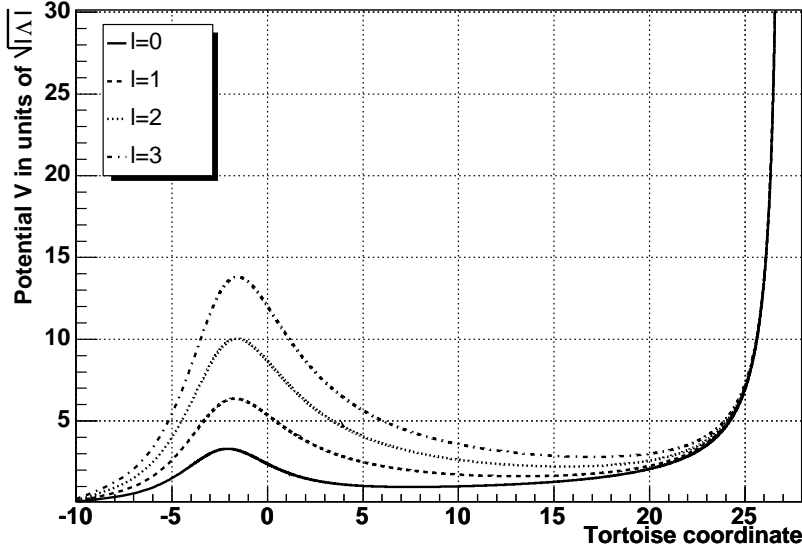


Figure 7: The potential in units of  $\sqrt{|\Lambda|}$  seen by a massless scalar field in SAdS space-time as a function of the tortoise coordinate for  $r_H = 0.1$  and for  $\eta \ll 1$ .

## 5.2 Stationary states solutions

The solution being developed in stationary states  $\psi(r^*, t) = \psi_r(r^*)e^{-i\omega t}$ , the equation of motion is given by Eq. (6) where  $\omega$  is a real and positive parameter. The WKB solutions depends on the energy<sup>2</sup>  $\omega$  of the field and the problem has to be divided into three energy regimes, defined by the number of classical turning points : i)  $\omega < V_{\min}^{(\ell)}$  (Regime I), one turning point  $r_-$  located before  $r_{\max}^{(\ell)}$  ; ii)  $V_{\min}^{(\ell)} < \omega < V_{\max}^{(\ell)}$  (Regime II), three turning points,  $r_{\pm}$  corresponding to the potential barrier induced by the black hole and  $r_0$  corresponding to the infinite barrier at spatial infinity ; iii)  $V_{\max}^{(\ell)} < \omega$  (Regime III), one turning point  $r_0$  which also corresponds to the infinite potential barrier. The boundary conditions, although depending on the considered quantity (quasi-normal frequencies, greybody factors, *etc.*), should read as follows in the most general case :

$$\psi_r(r^*) \rightarrow \begin{cases} \frac{A_{in}}{\sqrt{\omega}} e^{-i\omega r^*} + \frac{A_{out}}{\sqrt{\omega}} e^{i\omega r^*} & \text{when } r^* \rightarrow -\infty \\ 0 & \text{when } r^* \rightarrow r_{\text{SAdS}}^* \end{cases} \quad (38)$$

Considering first the *one-turning-point* case, the WKB wave functions has to be considered

<sup>2</sup>Calling *energy* the frequency parameter  $\omega$  was meaningful in the previously studied space-times as it was corresponding to the energy of particles for observers located at  $r = 0$  in AdS Universe or at spatial infinity in Schwarzschild ones. Although such *flat* observers do not exist in SAdS background, we keep calling *energy* the frequency parameter to avoid using too many variables.

in two regions : i)  $r < r_{-/0}$  (Region  $\mathcal{A}$ ) where the solutions are progressive waves and ii)  $r > r_{-/0}$  (Region  $\mathcal{B}$ ) where the solutions are evanescent and exponentially divergent waves. With proper boundary conditions, the WKB wave functions are obtained by the matching procedure at  $r < r_{-/0}$  described in appendix A :

$$\psi_r(r^*) = \begin{cases} \frac{A_{out}}{\sqrt{p(r^*)}} \left( e^{i \int^{r^*} p(x) dx} - i e^{-i \int^{r^*} p(x) dx} \right) & \text{in Region } \mathcal{A} \\ \frac{A_{out}}{\sqrt{p'(r^*)}} e^{-i \frac{\pi}{4} - \int_{r_{-/0}^*}^{r^*} p'(x) dx} & \text{in Region } \mathcal{B}. \end{cases} \quad (39)$$

For the *three-turning-points* case, the WKB solutions are considered in four regions : i)  $r < r_-$  (Region  $\mathcal{A}$ ) where the solutions are progressive waves ; ii)  $r_- < r < r_+$  (Region  $\mathcal{B}$ ) where the solutions are evanescent and exponentially divergent waves ; iii)  $r_+ < r < r_0$  (Region  $\mathcal{C}$ ) where the solutions are also progressive waves and iiiii)  $r > r_0$  (Region  $\mathcal{D}$ ) where the solutions are only evanescent waves, taking into account the boundary conditions at  $r_{SAdS}^*$ . Applying the matching procedure, the WKB solutions are found to be :

$$\psi_r(r^*) = \begin{cases} \frac{A_{out}}{\sqrt{p(r^*)}} \left( e^{i \int^{r^*} p(x) dx} - i e^{-i \int^{r^*} p(x) dx} \right) & \text{in Region } \mathcal{A} \\ \frac{A_{out}}{\sqrt{p'(r^*)}} e^{-i \frac{\pi}{4} - \int_{r_-^*}^{r^*} p'(x) dx} & \text{in Region } \mathcal{B} \\ \frac{A_{out} e^{-\tau}}{2\sqrt{p(r^*)}} \left( e^{i \int^{r^*} p(x) dx} - i e^{-i \int^{r^*} p(x) dx} \right) & \text{in Region } \mathcal{C} \\ \frac{A_{out} e^{-\tau}}{2\sqrt{p'(r^*)}} e^{-i \frac{\pi}{4} - \int_{r_0^*}^{r^*} p'(x) dx} & \text{in Region } \mathcal{D}. \end{cases} \quad (40)$$

where  $\tau = \int_{r_-}^{r_+} p'(x) dx$ . This strange behaviour in Region  $\mathcal{B}$  arises because we have assumed that the solutions can be decomposed into stationary state and because of the semi-classical ansatz. When considering the shape of the potential, it is clear that the states in Region  $[r_{\max}^{(\ell)}, +\infty]$  cannot be stationary states but quasi-stationary ones, as tunneling transition from Region  $\mathcal{C}$  to Region  $\mathcal{A}$  is possible but not taken into account in a first order semi-classical expansion.

The radial density probability for scalar particles can be inferred from the above stationary state solutions and takes the following form :

$$\rho(r^*) = i \left[ \psi_r(r^*) e^{-i\omega t} \partial_t (\psi_r^\dagger(r^*) e^{i\omega t}) - \psi_r^\dagger(r^*) e^{i\omega t} \partial_t (\psi_r(r^*) e^{-i\omega t}) \right] = 2\omega \psi_r^\dagger(r^*) \psi_r(r^*). \quad (41)$$

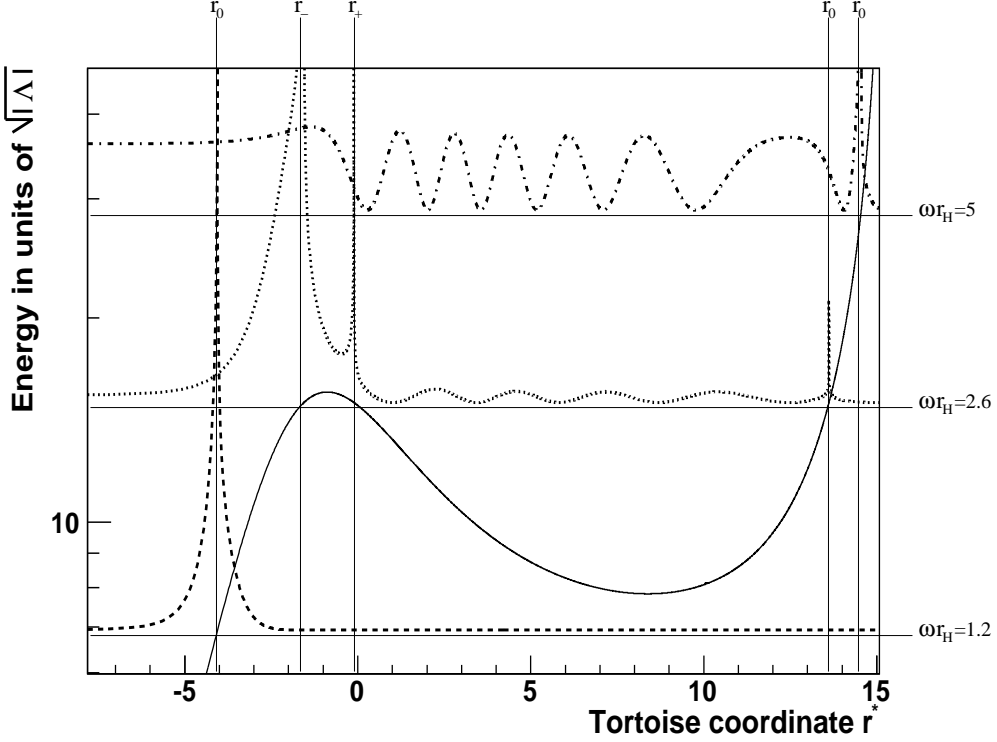


Figure 8: Probability densities as functions of  $r^*$  alongside the  $\ell = 6$  scalar potential (solid line) for  $\eta = 10$ : the dashed line stands for  $\omega < V_{\min}^{(\ell)}$ , the dotted line for  $V_{\min}^{(\ell)} < \omega < V_{\max}^{(\ell)}$  and the dotted-dashed line for  $\omega > V_{\max}^{(\ell)}$ . Each probability is displayed at its energy  $\omega_i$ , the horizontal line at  $\omega = \omega_i$  corresponding to  $\rho = 0$ . The turning-points are shown and the energy can be inferred either in units of  $\sqrt{|\Lambda|}$  on the left  $y$ -axis or in units of  $r_H^{-1}$  on the right.

In the three-turning-points case, the density probability therefore reads as

$$\rho(r^*) = 2\omega |A_{out}|^2 \begin{cases} \frac{2}{p(r^*)} \left[ 1 + \cos \left( 2 \int_{r^*}^{r_+} p(x) dx + \frac{\pi}{2} \right) \right] & \text{in Region } \mathcal{A} \\ \frac{1}{p'(r^*)} \exp \left( -2 \int_{r_+}^{r^*} p'(x) dx \right) & \text{in Region } \mathcal{B} \\ \frac{e^{-2\tau}}{2p(r^*)} \left[ 1 + \cos \left( 2 \int_{r_+}^{r^*} p(x) dx + \frac{\pi}{2} \right) \right] & \text{in Region } \mathcal{C} \\ \frac{e^{-2\tau}}{4p'(r^*)} \exp \left( -2 \int_{r_0}^{r^*} p'(x) dx \right) & \text{in Region } \mathcal{D}. \end{cases} \quad (42)$$

This probability is displayed on Fig. 8 for three different cases. As expected, at the turning points, the probability density diverges because of the  $p^{-1}(r^*)$  factor, which is a direct consequence of the breakdown of the WKB approximation. Since the potential rapidly falls down to zero, the radial probability density rapidly tends to the coherent superposition of incoming and outgoing free particles, *i.e.* plane waves, with the same amplitude  $\lim_{r^* \rightarrow -\infty} \rho(r^*) = \frac{1}{2} [1 + \cos(2\omega r^* + \frac{\pi}{2} + \varphi(r_{ini}^*))]$ , where  $\varphi$  is an additional phase depending on the initial posi-

tion chosen for integration. The minimum and maximum energy cases can be divided into two parts : before the turning point, the probability density is described by interferences between ingoing and outgoing modes, whereas after the turning point the probability density is a decreasing exponential which falls down to zero at  $r^* = r_{\text{SAdS}}^*$ . For the intermediate energy case, the space is separated into four regions : for  $r < r_-$  and  $r_+ < r < r_0$ , the probability density takes the form of interferences between ingoing and outgoing modes whereas it takes the form of a decreasing exponential in the  $r_- < r < r_+$  and  $r > r_0$  regions and falls down to zero at  $r^* = r_{\text{SAdS}}^*$ .

Some conclusions about the black hole evaporation process with a negative cosmological constant can be inferred in this framework. As in SdS space-time, the evaluation of the transmission coefficient critically depends upon the position of the observer. If the observer is located at spatial infinity, the transmission coefficient falls down to zero because of the total reflexion at  $r_0$ . However, this can be avoided by considering an observer near the local minimum, which is always possible in the case of a high hierarchy. Particles with an energy lying in Regime I are then totally reflected at  $r_-$  and the observer should not see any particle with an energy lower than  $V_{\text{min}}^{(0)}$  coming from the black hole. In addition, for quanta with  $\omega > V_{\text{min}}^{(0)}$ , only modes with angular momentum lower than  $m$ , so that  $V_{\text{min}}^{(m-1)} < \omega < V_{\text{min}}^{(m)}$ , can reach the observer. For  $\omega < V_{\text{max}}^{(\ell)}$ , the transmission coefficient is given by  $e^{-2\tau}$  while it becomes equal to one for particles with  $\omega > V_{\text{max}}^{(\ell)}$ . The qualitative features of the evaporation process of SAdS black holes can therefore be captured. It should, of course, be pointed out that a realistic study of this phenomenon has to be carried out dynamically, involving a full resolution of the KG equation while keeping the time dependence.

### 5.3 Energy levels and bandwidths

Because of the shape of the SAdS potential, the density of states for scalar fields is smooth and continuous with some resonances at specific energies, lying in the  $[V_{\text{min}}, V_{\text{max}}]$  range, with bandwidths given by the tunnel probabilities. This should lead to stationary states when the potential barrier becomes either infinitely large or infinitely high. The aforementioned conditions can be obtained for high angular momentum quantum numbers as well as for a vanishing  $\eta$  ratio. Working at the semi-classical order, the energy levels are computed by

	$n = 0$	$n = 1$	$n = 2$	$n = 3$
$\ell = 0$	$2.49 - i0.24$	$4.51 - i0.44$	$6.52 - i0.63$	$8.53 - i0.83$
$\ell = 1$	$3.82 - i0.02$	$5.82 - i0.04$	$7.82 - i0.05$	$9.82 - i0.07$
$\ell = 2$	$4.86 - i1.6 \cdot 10^{-3}$	$6.86 - i2.3 \cdot 10^{-3}$	$8.86 - i3.0 \cdot 10^{-3}$	$10.85 - i3.7 \cdot 10^{-3}$
$\ell = 3$	$5.88 - i9.0 \cdot 10^{-5}$	$7.88 - i1.2 \cdot 10^{-4}$	$9.88 - i1.5 \cdot 10^{-4}$	$11.87 - i1.8 \cdot 10^{-4}$
$\ell = 4$	$6.88 - i4.6 \cdot 10^{-6}$	$8.88 - i6.0 \cdot 10^{-6}$	$10.88 - i7.3 \cdot 10^{-6}$	$12.88 - i8.7 \cdot 10^{-6}$
$\ell = 5$	$7.89 - i2.3 \cdot 10^{-7}$	$9.89 - i2.9 \cdot 10^{-7}$	$11.88 - i3.5 \cdot 10^{-7}$	$13.88 - i4.1 \cdot 10^{-7}$

Table 1: Complex energy levels ( $\nu_{n,\ell} \times R$ ) for  $\eta = 5 \times 10^{-4}$  as functions of the angular momentum quantum number  $\ell$  and the integer  $n$  of the Bohr-Sommerfeld quantization rule.

solving numerically the following algebraic equation :

$$2 \int_{r_+}^{r_0} \frac{\sqrt{\omega_{n,\ell}^2 - V_\ell^2(r)}}{h(r)} dr - (2n + 1) \pi = 0, \quad (43)$$

where  $\omega_{n,\ell}^2$  stands for the unknown quantity. Unlike the AdS case, the usual radial coordinate  $r$  is preferred over the tortoise one. The numerical investigations show that, at the semi-classical order, the product  $\omega_{n,\ell} \times R$  only depends on the ratio  $\eta$ ,  $(n, \ell)$  being fixed. Consequently, the energy levels can be written in a very convenient way :  $\omega_{n,\ell} \times R \approx f(n, \ell) \times g(\eta)$ , where  $f$  and  $g$  are two functions which respectively depend on  $(n, \ell)$  and  $\eta$ . The bandwidth  $\Gamma$  of the resonances is given by the product of the tunnel probability  $|A_\ell|^2$  with the number of collisions at the turning point  $r_+$  :  $\Gamma_{n,\ell} = \omega_{n,\ell} \times |A_\ell|^2$ , with  $|A_\ell|^2$  given by

$$|A_\ell|^2 = \begin{cases} \exp \left( -2 \int_{r_-}^{r_+} \frac{\sqrt{V_\ell^2 - \omega_{n,\ell}^2}}{h(r)} dr \right) \\ \left( 1 + \exp \left( -2\pi p^2(r_{\max}) \left( 2 \frac{d^2 p^2}{dr^2}(r_{\max}) \right)^{-1/2} \right) \right)^{-1}. \end{cases} \quad (44)$$

In view of the results obtained for the greybody factors, the second WKB tunnel probability should be preferred as it provides more accurate results. The numerical investigations lead to assume that this bandwidth can also be separated into a  $(n, \ell)$  dependence and a  $\eta$  dependence, as in the case of the resonant energy position.

The semi-classical characteristics of resonances numerically obtained are presented in Tables 1 to 4 for four different values of the ratio  $\eta = \{0.0005, 0.001, 0.01, 0.1\}$  corresponding to cases where the finite potential barrier appears at any multipolar order. The tables give the complex energy  $\nu_{n,\ell} = \omega_{n,\ell} - i\Gamma_{n,\ell}$  in units of  $R^{-1}$ . As the KG equation is solved with the ansatz  $\Psi = e^{-i\nu t} Y_\ell^m(\Omega) R(r)$ , the imaginary part of the complex energy has to be negative.

	$n = 0$	$n = 1$	$n = 2$	$n = 3$
$\ell = 0$	$2.51 - i0.24$	$4.54 - i0.44$	$6.55 - i0.64$	$8.56 - i0.83$
$\ell = 1$	$3.83 - i0.027$	$5.82 - i0.042$	$7.82 - i0.057$	$9.81 - i0.071$
$\ell = 2$	$4.86 - i1.6 \cdot 10^{-3}$	$6.86 - i2.3 \cdot 10^{-3}$	$8.86 - i3.0 \cdot 10^{-3}$	$10.85 - i3.7 \cdot 10^{-3}$
$\ell = 3$	$5.88 - i9.0 \cdot 10^{-5}$	$7.87 - i1.2 \cdot 10^{-4}$	$9.87 - i1.5 \cdot 10^{-4}$	$11.87 - i1.8 \cdot 10^{-4}$
$\ell = 4$	$6.88 - i4.6 \cdot 10^{-6}$	$8.88 - i6.0 \cdot 10^{-6}$	$10.88 - i7.4 \cdot 10^{-6}$	$12.88 - i8.7 \cdot 10^{-6}$
$\ell = 5$	$7.89 - i2.3 \cdot 10^{-7}$	$9.89 - i2.9 \cdot 10^{-7}$	$11.89 - i3.5 \cdot 10^{-7}$	$13.88 - i4.1 \cdot 10^{-7}$

Table 2: Complex energy levels ( $\nu_{n,\ell} \times R$ ) for  $\eta = 10^{-3}$  as functions of the angular momentum quantum number  $\ell$  and the integer  $n$  of the Bohr-Sommerfeld quantization rule.

	$n = 0$	$n = 1$	$n = 2$	$n = 3$
$\ell = 0$	$2.61 - i0.26$	$4.64 - i0.47$	$6.63 - i0.70$	$8.62 - i0.97$
$\ell = 1$	$3.82 - i0.028$	$5.79 - i0.044$	$7.77 - i0.060$	$9.74 - i0.079$
$\ell = 2$	$4.85 - i1.7 \cdot 10^{-3}$	$6.83 - i2.4 \cdot 10^{-3}$	$8.81 - i3.2 \cdot 10^{-3}$	$10.78 - i4.1 \cdot 10^{-3}$
$\ell = 3$	$5.87 - i9.2 \cdot 10^{-5}$	$7.85 - i1.2 \cdot 10^{-4}$	$9.83 - i1.6 \cdot 10^{-4}$	$11.80 - i2.0 \cdot 10^{-4}$
$\ell = 4$	$6.88 - i4.8 \cdot 10^{-6}$	$8.86 - i6.2 \cdot 10^{-6}$	$10.84 - i7.7 \cdot 10^{-6}$	$12.82 - i9.3 \cdot 10^{-6}$
$\ell = 5$	$7.88 - i2.4 \cdot 10^{-7}$	$9.87 - i3.0 \cdot 10^{-7}$	$11.85 - i3.7 \cdot 10^{-7}$	$13.83 - i4.4 \cdot 10^{-7}$

Table 3: Complex energy levels ( $\nu_{n,\ell} \times R$ ) for  $\eta = 10^{-2}$  as functions of the angular momentum quantum number  $\ell$  and the integer  $n$  of the Bohr-Sommerfeld quantization rule.

	$n = 0$	$n = 1$	$n = 2$	$n = 3$
$\ell = 0$	$2.65 - i0.75$	/	/	/
$\ell = 1$	$3.6 - i0.12$	$5.4 - i0.95$	/	/
$\ell = 2$	$4.74 - i8.6 \cdot 10^{-3}$	$6.52 - i0.055$	$8.22 - i0.459$	$9.81 - i3.42$
$\ell = 3$	$5.77 - i5.5 \cdot 10^{-4}$	$7.58 - i2.8 \cdot 10^{-3}$	$9.34 - i0.019$	$11.03 - i0.15$
$\ell = 4$	$6.79 - i3.4 \cdot 10^{-5}$	$8.62 - i1.5 \cdot 10^{-4}$	$10.41 - i8.2 \cdot 10^{-4}$	$12.15 - i5.5 \cdot 10^{-3}$
$\ell = 5$	$7.80 - i2.0 \cdot 10^{-6}$	$9.65 - i8.3 \cdot 10^{-6}$	$11.46 - i3.9 \cdot 10^{-5}$	$13.23 - i2.2 \cdot 10^{-4}$

Table 4: Complex energy levels ( $\nu_{n,\ell} \times R$ ) for  $\eta = 10^{-1}$  as functions of the angular momentum quantum number  $\ell$  and the integer  $n$  of the Bohr-Sommerfeld quantization rule.

The positions of resonances tend to the pure AdS energy spectrum when  $\eta$  tends to zero for all angular momenta except when  $\ell = 0$ . This is not surprising since, for SAdS space-times, an infinite steepness of the wall never arises, even for arbitrarily small black holes : the transition from AdS to SAdS space-times is singular.

The bandwidth of the resonances behaves as expected : on the one hand, either a decrease of  $\eta$  or an increase of  $\ell$  leads to a decrease of the bandwidth since the well-potential is deeper and, on the other hand, the bandwidth becomes larger for higher values of  $n$  because of the increasing tunnel probability. Finally, when  $\eta \rightarrow 0$ , the quasi-stationary states tend to the stationary ones of an AdS Universe except for a vanishing angular momentum quantum number. The specific behaviour of the monopole partial waves underlines the singular behaviour of the SAdS scalar potential. However, it cannot be excluded that this arises from the use of semi-classical methods and is only an artifact of this approximated scheme.

## 6 Conclusions and perspectives

It was shown in this article that semi-classical methods for the resolution of Schrödinger-like equations can be successfully applied to scalar fields propagating in a static, spherically symmetric, curved background. The radial part of the KG equation has to be rewritten in a more convenient in a systematic scheme : the tortoise coordinate is used and the unknown function is redefined independently of the metric. The propagation of fields is then described by a 1-dimensional Schrödinger equation whose resolution can be performed with a semi-classical ansatz. However, the classical problem underlying the quantum one is based on a slightly-modified-from-relativistic-case Hamilton-Jacobi equation where what is usually interpreted as the potential is here seen as the square of the potential. The semi-classical method was then used to study the behaviour of scalar fields in AdS and Schwarzschild backgrounds and it was shown that the energy levels in an AdS universe and the greybody factors entering the Hawking radiation law are both recovered at the semi-classical order with a very good accuracy. It should also be emphasized that the WKB estimation of the greybody factors provides a powerful tool for theoretical investigations, *i.e* for testing the influence of a given space-time curvature on the emission/absorption cross-sections. Finally, we have performed a semi-classical study of scalar fields propagating in SAdS space-times. The potential seen by those fields imposes resonances in the density of states, whose positions in energy and bandwidths can be evaluated using the



Bohr-Sommerfeld quantization rule for the former quantity and the WKB tunnel probability for the latter one.

In principle, all the above results could be improved : first, the Taylor expansion of the ansatz used in the KG equation could be preformed up to higher orders. Then, as it has already been mentioned by Langer [3], considering the radial part of the Schrödinger equation as a one dimensional equation remains a naive approach as the centrifugal potential exhibits a singular behaviour when  $r \rightarrow 0$ . As discussed in [15], the phase of the WKB wave function for radial motion does not match the one of the exact wave function in regions where the potential can be neglected when compared to the centrifugal one. Nevertheless, the matching between both solutions can still be performed by replacing  $\ell(\ell + 1)$  by  $(\ell + 1/2)^2$  but, in any case, a precise study of the matching between the semi-classical wave functions and the exact ones, in regions where such exact solutions can be found, have to be carried out before applying the *Langer trick*.

Finally, the semi-classical methods provide a powerful tool to study the dynamics of scalar fields in curved space-times as, in most cases, exact solutions cannot be derived. As an example, the highly non-trivial problem of the Hawking evaporation process for SAdS black holes can be greatly simplified in this way and is currently the only available treatment. Another field of application is related to primordial cosmology where the WKB approach, first used by Martin & Schwarz [5], has been extended to the second order by the authors of Ref. [6] so as to derive the primordial fluctuations power spectrum. However, it has been recently proven by the authors of Ref. [29] that the accuracy of the WKB approximation is intrinsically limited because it involves divergent series. This result, demonstrated in the case of cosmological particle production during the inflationary era, enlightens the cautious needed when dealing with WKB techniques.

#### **Acknowledgements:**

J.G. would like to thank P. Kanti for solving the KG equation in AdS background as well as L. Derome and K. Protasov for very helpful discussions.

## A Appendix A: Matching procedure

The matching procedure involves the equation  $\frac{d^2\psi}{d\xi^2} + p^2(\xi)\psi(\xi) = 0$  with two turning point at  $\xi_1$  and  $\xi_2$ . The procedure consists in restricting the momentum at the linear order  $p^2(\xi) \simeq -\lambda(\xi - \xi_1)$ , with  $\lambda > 0$ , and to match the new solutions with the WKB ones on the left and on the right of the turning point [5, 3, 15]. With this *linearized* momentum, the solution of the previous equation are expressed in terms of Airy functions ( $\mathbf{Ai}, \mathbf{Bi}$ ) :  $\psi(\xi) = B_1 \mathbf{Ai}\left(\lambda^{\frac{1}{3}}(\xi - \xi_1)\right) + B_2 \mathbf{Bi}\left(\lambda^{\frac{1}{3}}(\xi - \xi_1)\right)$ . As  $\xi$  is close to  $\xi_1$ , this solution can be expanded in terms of exponential:

$$\psi(\xi) = \begin{cases} \frac{\lambda^{-\frac{1}{12}}}{2\sqrt{\pi}} |\xi - \xi_1|^{-\frac{1}{4}} \left[ (B_2 - iB_1) \exp\left(i\frac{2}{3}\sqrt{\lambda}|\xi - \xi_1|^{\frac{3}{2}} + i\frac{\pi}{4}\right) \right. \\ \left. + (B_2 + iB_1) \exp\left(-i\frac{2}{3}\sqrt{\lambda}|\xi - \xi_1|^{\frac{3}{2}} - i\frac{\pi}{4}\right) \right] & \text{in region } \mathcal{A} \\ \frac{\lambda^{-\frac{1}{12}}}{\sqrt{\pi}} |\xi - \xi_1|^{-\frac{1}{4}} \left[ \frac{B_1}{2} \exp\left(-\frac{2}{3}\sqrt{\lambda}|\xi - \xi_1|^{\frac{3}{2}}\right) \right. \\ \left. + B_2 \exp\left(\frac{2}{3}\sqrt{\lambda}|\xi - \xi_1|^{\frac{3}{2}}\right) \right] & \text{in region } \mathcal{B}. \end{cases} \quad (45)$$

To perform the matching between Airy functions solutions and the WKB solutions, we calculate the WKB solutions in the two region using the linear approximation for the momentum :

$$\psi(\xi) = \begin{cases} \lambda^{-\frac{1}{4}} |\xi - \xi_1|^{-\frac{1}{4}} \left[ A_{out} \exp\left(-i\frac{2}{3}\sqrt{\lambda}|\xi - \xi_1|^{\frac{3}{2}}\right) \right. \\ \left. + A_{in} \exp\left(i\frac{2}{3}\sqrt{\lambda}|\xi - \xi_1|^{\frac{3}{2}}\right) \right] & \text{in region } \mathcal{A} \\ \lambda^{-\frac{1}{4}} |\xi - \xi_1|^{-\frac{1}{4}} A_{eva} \exp\left(-\frac{2}{3}\sqrt{\lambda}|\xi - \xi_1|^{\frac{3}{2}}\right) & \text{in region } \mathcal{B}. \end{cases} \quad (46)$$

Matching  $B_{1/2}$  to  $A_{out/in}$  and to  $A_{eva/div}$ , it is possible to match the two solutions in regions  $\mathcal{A}$  and  $\mathcal{B}$  :  $A_{eva} = e^{-i\frac{\pi}{4}} A_{out}$  and  $A_{in} = e^{-i\frac{\pi}{2}} A_{out}$ .

The same procedure is applied at the second turning point  $\xi_2$  just by introducing  $\xi' = -\xi$ , at this point the WKB solutions take the form :

$$\psi(\xi') = \begin{cases} \lambda^{-\frac{1}{4}} |\xi' - \xi_2|^{-\frac{1}{4}} A_{eva} e^{-\tau} \exp\left(\frac{2}{3}\sqrt{\lambda}|\xi' - \xi_2|^{\frac{3}{2}}\right) & \text{in region } \mathcal{B} \\ \lambda^{-\frac{1}{4}} |\xi' - \xi_2|^{-\frac{1}{4}} B_{out} \exp\left(i\frac{2}{3}\sqrt{\lambda}|\xi' - \xi_2|^{\frac{3}{2}}\right) & \text{in region } \mathcal{C} \end{cases} \quad (47)$$

with  $\tau = \int_{r_1^*}^{r_2^*} p'(\xi) d\xi$  and gives:  $B_{out} = e^{i\frac{\pi}{4}} e^{-\tau} A_{eva}$ . From this equation and the previous one, we finally obtain the amplitude of the outgoing waves at  $+\infty$  in function of the amplitude of

the outgoing waves at  $-\infty$ :  $B_{out} = e^{-\tau} A_{out}$ .

## B Appendix B: Resolution of the AdS-KG equation

To solve [9] the differential Eq. (19), a change of variable as well as a change of the unknown function is performed :  $z = \cos(2\rho)$  ;  $R(\rho) = \sin^\ell(\rho) \cos^\beta(\rho) P(\rho)$ . Under this change, the differential equation is of the form [19]  $(1-z^2) \frac{d^2 P}{dz^2} + (b-a-(a+b+2)z) \frac{dP}{dz} + n(n+a+b+1)P(z) = 0$  where the parameters  $(\beta, a, b, n)$  must satisfy the four constraints :

$$a + b + 2 = \ell + 1 + \beta ; b - a = \beta - 2 - \ell ; \beta(\beta - 3) = 0 ; n(n + a + b + 1) = \frac{1}{4} (\nu^2 - (\ell + \beta)^2). \quad (48)$$

The solution are the Jacobi's polynomials  $P_n^{(a,b)}(z)$ , imposing that  $n$  is an integer,  $a > -1$  and  $b > -1$  [19]. Once the four constraints for the parameters  $(\beta, a, b, n)$  solved, the solution of the radial part of the KG equation is expressed in function of the Jacobi's polynomials :  $R(\rho) = \sin^\ell(\rho) \cos^3(\rho) P_{(\nu-\ell-3)/2}^{(\ell+1/2, 3/2)}(\cos(2\rho))$  where we choose  $\beta = 3$  in order to respect the  $b > -1$  constraint.

## C Appendix C: Determination of the turning points

In the  $\ell \neq 0$  case, the determination of  $r_\pm^*$  is more complicated. Introducing  $y = \tan(r^*/R)$ , the solutions of the equation  $\omega = V(r)$  are given by the algebraic equation  $2y^4 + (2 + \ell(\ell + 1) - \omega^2 R^2) y^2 + \ell(\ell + 1) = 0$ . In order to have two different, positive, real roots, three constraints have to be satisfied:

$$\begin{aligned} 2 + \ell(\ell + 1) - \omega^2 R^2 &\leq 0 \\ (2 + \ell(\ell + 1) - \omega^2 R^2)^2 - 8\ell(\ell + 1) &\geq 0 \\ 8\ell(\ell + 1) &\geq 0 \end{aligned} \quad (49)$$

where the third one is always satisfied. Solving the first constraint, the zero-point energy feature of the energy spectrum is recovered  $\omega \geq \frac{1}{R} \sqrt{2 + \ell(\ell + 1)}$ . This result is in good agreement with the exact energy spectrum as  $\sqrt{2 + \ell(\ell + 1)} < \ell + 3$ . Under such constraints, only two positive, real roots exist which are the two turning points:

$$y_\pm = \frac{1}{2} \sqrt{\omega^2 R^2 - 2 - \ell(\ell + 1) \pm \sqrt{(2 + \ell(\ell + 1) - \omega^2 R^2)^2 - 8\ell(\ell + 1)}}. \quad (50)$$

## References

- [1] H. A. Kramers, *Z. Phys.* **39** (1926) 836.
- [2] L. A. Young and G. E. Uhlenbeck, *Phys. Rev.* **36** (1930) 1158.
- [3] R. E. Langer, *Phys. Rev.* **51** (1937) 669.
- [4] M. K. Parikh and F. Wilczek, *Phys. Rev. Lett.* **85** (2000) 5042.
- [5] J. Martin and D. J. Schwarz, *Phys. Rev. D* **67** (2003) 083512.
- [6] R. Casadio, F. Finelli, M. Luzzi, G. Venturi *Phys. Rev D* 71 (2005) 043517; R. Casadio, F. Finelli, M. Luzzi, G. Venturi *Phys. Lett. B* 625 (2005) 1; R. Casadio, F. Finelli, M. Luzzi, G. Venturi **gr-qc/0510103**
- [7] H. P. Nollert, *Class. Quantum Grav.* **16** (1999) R159.
- [8] C. P. Burgess and C. A. Lutken, *Phys. Lett. B* **153** (1985) 137; I. I. Cotaescu, *Phys. Rev. D* **60** (1999) 107504.
- [9] P. Kanti, *private communication*.
- [10] A. S. Cornell, W. Naylor and M Sasaki, **hep-th/0510009**.
- [11] B. F. Schutz and C. M. Will, *Ap. J* **291** (1985) L33; S. Iyer and C. M. Will, *Phys. Rev. D* **35** (1987) 3621; R. A. Konoplya, *Phys. Rev. D* **68** (2003) 024018; R. A. Konoplya, *Phys. Rev. D* **71** (2005) 024038; E. Abdalla, R. A. Konoplya and C. Molina, **hep-th/0507100**.
- [12] V. Cardoso, R. Konoplya & J. P. S. Lemos, *Phys. Rev. D* **68** (2003) 044024, T. R. Govindarajan & V. Suneeta, *Class. Quantum Grav.* **18** (2001) 265
- [13] V.P. Frolov and I. D. Novikov, *Black Holes Physics: Basic Concepts and New Developments* (Kluwer Academic Publishers, 1998).
- [14] S. Chandrasekhar, *The Mathematical Theory of Black Holes* (Oxford University Press, New York, 1983).
- [15] M. Brack and R. K. Bhaduri, *Semiclassical Physics* (Addison-Wesley Publishing Company, Inc., 1997).
- [16] A. Messiah, *Mécanique Quantique* (Dunod, Paris, 1965).

- [17] S. W. Hawking and G. Ellis, *The Large Scale Structure of Space-time* (Cambridge Univ. Press, London, 1973).
- [18] S. J. Avis, C. J. Isham and D. Storey, Phys. Rev. D **18** (1978) 3565.
- [19] M. Abramowitz and I. A. Stegun, *Handbook of Mathematical Functions* (Dover Publication Inc., New York, 1966).
- [20] W. H. Press, S. A. Teukolsky, W. T. Vetterling and B. P. Flannery, *Numerical Recipes* (Cambridge University Press, Cambridge, 1988).
- [21] S. W. Hawking, Commun. Math. Phys. **43** (1975) 199.
- [22] D. N. Page, Phys. Rev. D **13** (1976) 198; D. N. Page, Phys. Rev. D **14** (1976) 1509; D. N. Page, Phys. Rev. D **16** (1977) 2402.
- [23] J. J. Sakurai, *Modern Quantum Mechanics* (Addison-Wesley Publishing Company, Inc., 1994).
- [24] C. M. Harris and P. Kanti, JHEP **310** (2003) 014; C. M. Harris and P. Kanti, **hep-th/0503010**; G. Duffy, C. M. Harris, P. Kanti and E. Winstanley **hep-th/0507274**.
- [25] P. Kanti, J. Grain and A. Barrau, Phys. Rev. D **71** (2005) 104002.
- [26] J. Grain, A. Barrau and P. Kanti, Phys. Rev. D **72** (2005) 104016.
- [27] P. Kanti and J. March-Russell, Phys. Rev. D **66** (2002) 024023; P. Kanti and J. March-Russell, Phys. Rev. D **67** (2003) 104019.
- [28] P. Kanti, Int. J. Mod. Phys. **A19** (2004) 4899.
- [29] S. Winitzki, Phys. Rev. D **72** (2005) 104011